Biosensors and Bioelectronics 127 (2019) 207–214

Contents lists available at ScienceDirect

Biosensors and Bioelectronics

journal homepage: www.elsevier.com/locate/bios

A robust electrochemical sensing of molecularly imprinted polymer prepared by using bifunctional monomer and its application in detection of cypermethrin

Yangguang Li[a,1], Lu Zhang[b,1], Yanyan Dang[a], Zongqin Chen[d], Ruyue Zhang[e], Yingchun Li[b,*], Bang-Ce Ye[a,c,**]

[a] Key Laboratory for Green Processing of Chemical Engineering of Xinjiang Bingtuan, School of Chemistry and Chemical Engineering, Shihezi University, Shihezi, China
[b] College of Science, Harbin Institute of Technology, Shenzhen 518055, China
[c] State Key Laboratory of Bioreactor Engineering, East China University of Science and Technology, Shanghai 200237, China
[d] Shihezi University Normal College, China
[e] Key Laboratory of Xinjiang Phytomedicine Resource and Utilization, Ministry of Education, Shihezi University, Shihezi 832000, China

ARTICLE INFO

Keywords:
Ag and N co-doped zinc oxide
Response surface method
Activated carbon
Dual functional monomers
Molecularly imprinted polymer
Electrochemical sensor

ABSTRACT

This work describes a hybrid electrochemical sensor for highly sensitive detection of pesticide cypermethrin (CYP). Firstly, Ag and N co-doped zinc oxide (Ag-N@ZnO) was produced by sol-gel method, and then Ag-N@ZnO was ultrasonically supported on activated carbon prepared from coconut husk (Ag-N@ZnO/CHAC). Finally, a layer of molecularly imprinted polymer (MIP) was in situ fabricated on glassy carbon electrode by electropolymerization, with dopamine and resorcinol as dual functional monomers (DM), CYP acting as template (DM-MIP-Ag-N@ZnO/CHAC). Morphological features, composition information and electrochemical properties of DM-MIP-Ag-N@ZnO/CHAC were investigated in detail. It is worth to mention that for the first time response surface method was used to investigate the effect of double monomers and to optimize the ratio between template and monomers. Compared with typical one-monomer involving MIP, the MIP prepared with dual functional monomers (DMMIP) of monomers showed higher response and better selectivity. Under the optimal conditions, a calibration curve of current shift versus concentration of CYP was obtained in the range of 2×10^{-13}~8×10^{-9} M, and the developed sensor gave a remarkably low detection limit (LOD) of 6.7×10^{-14} M (S/N = 3). Determination of CYP in real samples was conducted quickly and accurately with our sensor. The DMMIP-Ag-N@ZnO/CHAC electrochemical sensor proposed in this paper has great potential in food safety, drug residue determination and environmental monitoring.

1. Introduction

Cypermethrin (CYP) is a kind of pesticides artificially synthesized by simulating the chemical structure of natural pyrethrin (Tang et al., 2017). It is widely used in agricultural production as well as for domestic purposes because of its broad spectrum, high efficiency and fast-acting characteristics (Shafer et al., 2005). However, in recent years, it has been found that pyrethroid pesticides may adversely affect the central nervous system and have endocrine disrupting effects that are highly toxic to mammals and aquatic organisms (GóMez-Gimã©Nez et al., 2017). Thus, accurate determination of trace levels of CYP is necessary in many fields. Common ways for CYP detection include high performance liquid chromatography (HPLC) (West, 1997), gas chromatography-mass spectrometry (GC-MS), immunoassay, etc (Shin et al., 2018; West, 1997; Zhou et al., 2018). However, there are some of the problems limit their application, such as high turnaround time, tedious pretreatment, false positive reaction and high cost (Y.C. Li et al., 2016; Zhang et al., 2014), which prompts researchers to explore new and efficient methods for CYP assay.

Electrochemical sensor has advantages of simple preparation, convenient operation, low detection limit and high sensitivity. Compared with the above mentioned methods, it can monitor trace analytes

* Corresponding author.
** Corresponding author at: Key Laboratory for Green Processing of Chemical Engineering of Xinjiang Bingtuan, School of Chemistry and Chemical Engineering, Shihezi University, Shihezi, China.
E-mail addresses: liyingchun@hit.edu.cn (Y. Li), bcye@ecust.edu.cn (B.-C. Ye).
[1] The authors contributed equally to this work.

https://doi.org/10.1016/j.bios.2018.12.002
Received 29 August 2018; Received in revised form 3 December 2018; Accepted 3 December 2018
Available online 07 December 2018
0956-5663/

quickly and immediately in a facile manner (Ng and Khor, 2017). However, selectivity is an inherent bottleneck for sensor-based detection, which limits its application since existence of various interferants in a ubiquitous phenomenon in real sample analysis (Chen et al., 2018). Therefore, modification is almost imperative to afford sensor with selectivity. Various biomaterials including nucleic acid, protein, enzyme, etc. (Alvau et al., 2018; Ng and Khor, 2017; Wu et al., 2017), have been used as functional matrix to realize specific recognition towards target substances. In comparison, the artificially synthesized molecularly imprinted polymer (MIP), owing to its unique merits like good stability, simple preparation, low cost, and not easy to be affected by the environment, is able to serve as an ideal recognizer candidate for generation of specific sensing signals (Capoferri et al., 2018; C. Zhang et al., 2018; H. Zhang et al., 2018, Y. Zhang et al., 2015). Moreover, along with the use of electrochemical probes as electrical signal indicators, MIP-based sensors are independent on electrochemical activity of analyte and therefore gain wide application prospect (Gupta et al., 2016; Li et al., 2018; Y.C. Li et al., 2016; Wei et al., 2017). Molecularly imprinted electrochemical sensor is usually prepared by electrochemical polymerization method, which can subtly control the thickness of the polymer film, and the obtained imprinted membrane is stable and uniform. In most MIP preparation, only one type of functional monomer is involved (Y. Li et al., 2016; Y.C. Li et al., 2016). Studies have shown that MIPs prepared with two or more functional monomers exhibit better performance than those with only one monomer (Ramstroem et al., 1993; Wu et al., 2016), due to the complementary function and synergistic effect played by diverse monomers on molecular recognition. In particular, both selectivity and adsorption capacity of MIPs can be elevated to certain extent when carefully selected dual monomers are involved in formation of polymeric skeleton, as the result of increase in polymer-template interaction categories and diversity of functional groups (Geng et al., 2014; Habaue et al., 2004; Zhao et al., 2017). In addition to the hydrogen bond between the carboxyl group and the pyridyl group, the difunctional monomer can interact with the template polymer through P-P. These monomers can effectively reflect the precise generation of templates, structures and chiral helical cavities (Habaue et al., 2004). It reminds us that employment of dual functional monomers could increase diversity of the types of blotting sites in MIP architecture and therefore enhance binding and affinity by synergistic effects of different monomers. As a result, the obtained dual-monomer MIP (DMMIP) can effectively enrich targets and eliminate interference, thus improving selectivity of MIP to imprinted molecules (Gui et al., 2018; Zhang and Li, 2018).

On the other hand, sensitivity is an ever-seeking feature in sensor development, for which various materials are used to modify sensor substrate in order to get enlarged sensing surface, including carbon materials, metal nanoparticles, metal oxides, (Kaur et al., 2017; Wang et al., 2017, 2018) Among them, activated carbon (AC) is very suitable for its low cost, easy availability and flourishing pore structure (Madhu et al., 2014). However, our pre-testing experiments implied that AC was liable to fall off when applied as a sensitizing material on electrode surface. It can not sustain continuous electrochemical scanning and thus can not be used directly as a bottom layer to load MIP film. Since AC alone has difficulty in forming rigid layer on electrode surface, which made us resort to composite materials for better immobilization. Metal oxides are expected to solve this issue due to their good compatibility with other materials (Li et al., 2017; Zhang et al., 2017; Alongi et al., 2010). As a common metal oxide, zinc oxide is low cost and exhibits outstanding optical, electrical and piezoelectrical properties. ZnO is a kind of low-cost and easy-preparation material, and exhibits outstanding optical, electrical and piezoelectrical properties. Also, ZnO can be easily integrated with other materials (Si et al., 2018; Suematsu et al., 2018; Naganathan et al., 2018), which makes it an efficient active agent in sensor application (Bougrine et al., 2003), including electrochemical sensor and photosensitive sensor. Doping is a common and efficient way to enhance electrical conductivity of ZnO and helps to extend its application in electrochemical sensing field (Ibrahim et al., 2015).

Therefore, our final strategy is to produce hybrid material by combining Ag-N@ZnO-loaded activated carbon (from coconut-shell biomass) with dual-monomer MIP and use it to construct an electrochemical sensor for detection of CYP. During MIP preparation, the response surface was employed to study the effect of double monomers and to optimize the ratio between template and monomers. What's more, we optimized the sweep speed, pH and incubation time, and the as prepared sensor was successfully used to detect CYP in crayfish, squid, soil and water samples.

2. Experimental part

2.1. Instruments and reagents

N, N-Dimethylformamide (DMF), ethanol, oxalic acid, dopamine (DA) resorcinol (RC) Fenpropathrin (FP) Deltamethrin (DM) Permethrin (PT) cypermethrin (CYP) were all purchased from Adamas Reagent Co. Ltd (Shanghai, China). Different grades of α-Al_2O_3 polishing powder were supplied by Sigma Aldrich Co (Titan, Shanghai), Zinc acetate and silver nitrate were obtained from Shanghai Future Reagent Co., Ltd. Reagents and materials, such as $K_3Fe(CN)_6$, $K_4Fe(CN)_6$, NaCl, $CHCl_3$, NH_4Cl, H_2SO_4, KNO_3, HNO_3, methanol, NaOH, acetonitrile and phosphate buffer (PB, KH_2PO_4 and K_2HPO_4), were of analytical level. All solutions were prepared using double distilled water and ultrasonicated by SY-360 Ultrasonic Cleaner (Shanghai Ningshang Ultrasonic Instrument Co., Ltd.). Activated carbon prepared from coconut shells was purchased from Tianjin Aida Hengyu Development Co., Ltd. Electrochemical measurements were carried out on a CHI 760E Electrochemical Workstation (Shanghai Chenhua Instrument Co., Ltd.) connected to a PC. The conventional three-electrode system includes a bare or modified planar glassy carbon electrode (GCE, 4 mm diameter) as the working electrode, a saturated calomel electrode (SCE) as the reference electrode and a platinum wire (0.5 mm in diameter and 34 mm in length) as the counter electrode, which were all purchased from Shanghai Chenhua Instrument Co., Ltd. Material morphology was characterized by a blue XFlash-SDD-5010 scanning electron microscope (Germany) at a voltage of 10 kV. The specific surface area of polymer was measured by using a Quantachrome NOVA 1000 based on the Brunauer-Emmett-Teller (BET) experiment. X-ray diffraction (XRD) patterns of all samples were analyzed using a Rigaku Giegerflex D/Max B diffractometer (Rigaku Corporation, Tokyo, Japan) with Cu-Kα radiation. The scanning step and velocity used was 0.02° and 0.01°/min, respectively, and the samples were scanned in the angle range of 10–80°. Surface composition and chemical states were conducted using X-ray photoelectron spectroscopy (XPS) (Thermo ESCALAB 250XI, Thermo Fisher Scientific, Waltham, MA, USA) equipped with a Mg Kα X-ray source (1253.6 eV) under a vacuum pressure less than 10^{-6} Pa. A centrifuge (Anke TGL-16G, Shanghai, China) was used in pretreatment of biological samples.

2.2. Synthesis of CHAC

First, coconut shells were fully ground and sifted by a 100-mesh sieve. The powder was washed with distilled water for 6–8 times, followed by drying at 110 °C for 8 h. Solid potassium hydroxide was then mixed with the powder and they were evenly mixed in a quartz tube at a mass ratio of 2.5:1. The mixture was heated in a microwave oven for 15 min with microwave power of 900 W. Finally, the obtained CHAC was dried after it was washed with deionized water until the filtrate was neutral.

2.3. Preparation of polymers Ag-N@ZnO/CHAC

The specific steps are as follows: 0.034 g silver nitrate, 2.196 g zinc

acetate and 0.9 g urea were dissolved in 60 mL absolute ethanol, and then stirred in a 60 °C water bath for 30 min, which was named as Solution A. Meanwhile, 5.04 g oxalic acid was stirred in 80 mL ethanol for 30 min and the obtained liquid was named as Solution B. The solution B was dropwise added into solution A, and then the mixture was stirred at room temperature for 1 h to obtain a sol. The sol was aged in a closed environment for 48 h to form homogeneous gel. The gel was dried in a vacuum oven at 80 °C for 24 h, and then heated in a 400 °C muffle furnace for 2 h to finally obtain Ag-N@ZnO. Preparation of ZnO was consistent with the above steps except that silver nitrate and zinc acetate were not added in solution A.

2.0 g activated carbon prepared from coconut shells was dispersed in 200 mL anhydrous ethanol for 1 h, and 0.20 g Ag-N@ZnO was dispersed in 50 mL anhydrous ethanol solution for 20 min. After that, the Ag-N@ZnO solution was mixed with the activated carbon solution and sonicated for 1 h, followed by stirring at 300 rpm for 15 h. Finally, the sample was suction filtered under vacuum and dried to obtain Ag-N@ZnO/CHAC. ZnO/CHAC was synthesized by using the same strategy.

2.4. Fabrication of electrochemical sensor

GCE was polished successively with 0.30 mm and 0.05 mm alumina powder, and then cleaned with distilled water. 5 mg Ag-N@ZnO/CHAC was suspended in DMF at the ratio of 1 mg mL^{-1}. 5 μL Ag-N@ZnO/CHAC suspension was dropped onto GCE surface and dried under infrared lamp for fabrication of Ag-N@ZnO/CHAC/GCE. MIP was synthesized via electro-polymerization in phosphate buffer containing 3×10^{-3} M CYP (as template) and 5×10^{-3} M resorcinol plus 3×10^{-3} M DA (both as functional monomer) by cyclic voltammetry (CV) carried out from 0 V to +0.8 V (vs. SCE) for 60 cycles at a scan rate of 50 mV s^{-1}. The electrode with the polymer film was immersed in 0.1 M NaOH to extract the embedded CYP (DMNIP-Ag-N@ZnO/CHAC/GCE) by scanning between −1.0 V and +1.0 V for 10 cycles until obvious and stable redox peaks could be observed in probe solution containing 0.1 M $[Fe(CN)_6]^{3-/4-}$ and 0.1 M KNO_3. The schematic representation for preparing DMMIP-Ag-N@ZnO/CHAC/GCE was illustrated in Fig. 1. For comparison, non-imprinted polymer (NIP) modified CYP electrode (DMNIP-Ag-N@ZnO/CHAC/GCE) was fabricated in the similar way except the participation of CYP.

2.5. Electrochemical measurements

CV was used to investigate the electrochemical behavior of different electrodes in probe solution. The change in peak current intensity produced by $Fe(CN)_6^{3-/4-}$ was used to evaluate the electrochemical performance of different sensors, as well as the binding of CYP or other substances. Detection procedure is as follows: The sensor was incubated in solution containing the analyte for 10 min and rinsed with distilled water to remove residual adherent surface material. After that, it was placed in probe solution and tested by CV. The electrochemical performance of the sensor was studied based on the difference (ΔI) of the reduction peak current before and after incubation in the test solution. After each detection, the electrode was placed in a 1.0 M NaOH solution, and the bound substance was removed by a few cycle in the range of −0.5 to +0.5 V using CV until a stable redox peak can be observed in probe solution. Then the recovered sensor is ready for the next analysis. Electrochemical impedance spectroscopy (EIS) experiments were carried out in solution containing 5 mM $[Fe(CN)_6]^{3-/4-}$ and 0.1 M KCl within a frequency range from 0.01 Hz to 100 kHz.

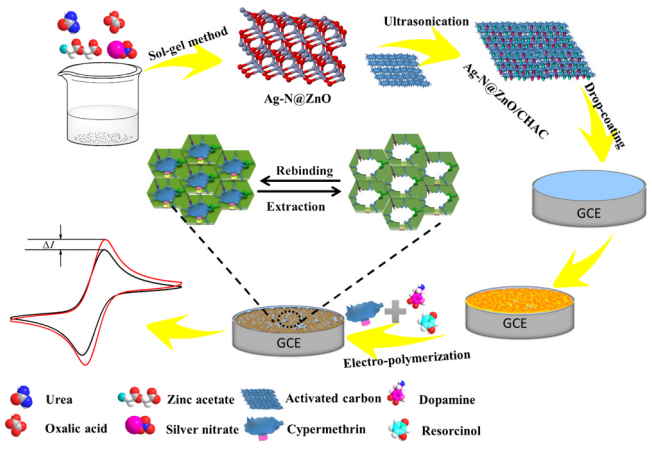

Fig. 1. Schematic preparation process of DMMIP-Ag-N@ZnO/CHAC/GCE.

2.6. Determination of cypermethrin in real samples

The sensor was used for determination of CYP in soil, mackerel, crayfish and water in order to verify its practical applicability. Particularly, mackerel and crucian carp purchased in the local market were fasted for 24 h, and CYP was mixed with feed and given three times a day (0.2 mg CYP per time). After feeding for two days, 2.0 g abdominal meat was collected and homogenized in a centrifuge tube containing 6 mL methanol. Thereafter, the sample was centrifuged at 8000 rpm for 10 min and the supernatant was diluted with an equal volume of methanol and centrifuged again at 5000 rpm for 10 min. The final supernatant was used for CYP detection. For the spiked recovery experiment, a certain amount of CYP was added in the biosamples during homogenization. The supernatant was stored at − 4 °C when not in use. As for soil analysis, the air-dried soil sample was ground with a pestle and sieved through 100 mesh. Afterwards, 5.0 g sample was dispersed in 30 mL methanol, and let stand for 1 h. After addition of a certain amount of CYP, the above mixture was centrifuged at 7000 rpm for 10 min and the obtained supernatant was collected for analysis Pretreatment of water samples was performed in the same way except for centrifugation.

3. Results and discussion

3.1. Characterization of polymers

Preparation of Ag-N@ZnO/CHAC is divided into two steps. First, Ag-N@ZnO was obtained by gelation method, and then Ag-N@ZnO was loaded on the surface of CHAC by ultrasonic agitation. After drop-coating of GCE with Ag-N@ZnO/CHAC, MIP film was synthesized in situ on the electrode surface via electropolymerization. Different materials and their composites were characterized, as well as the differently modified GCEs. Fig. 2A shows that ZnO is of nanorod structure with a side length of about 400 nm, and its morphology changes after Ag and N doping by forming irregular agglomerates (Fig. 2B). CHAC in Fig. 2C shows chain-like structure. When Ag-N@ZnO are loaded on the CHAC surface. It can be seen from Fig. 2D that the irregularly point-like Ag-N@ZnO is grafted on the strip of activated carbon. Compared with single CHAC, the width of the Ag-N@ZnO/CHAC chains increases and irregular aggregates are found on the surface. As shown in Fig. 2E, after electro-polymerization, the surface of Ag-N@ZnO/CHAC gets rougher and the width of pore size is reduced from ~50 nm to ~20 nm. These might be side notes implying successful preparation of MIP membrane which covers the surface of Ag-N@ZnO/CHAC evenly. Subsequent elution of the template molecule from the polymer network leads to enlarged surface porosity and pore size of MIP-Ag-N@ZnO/CHAC (Fig. 2F). BET diagrams of Ag-N@ZnO and Ag-N@ZnO/CHAC (Fig. 2G and H) display that the nitrogen adsorption/desorption isotherm of Ag-N@ZnO/CHAC is greater than that of Ag-N@ZnO, indicating that Ag-N@ZnO/CHAC has larger specific surface area (64.79 m^2 g^{-1}) than Ag-

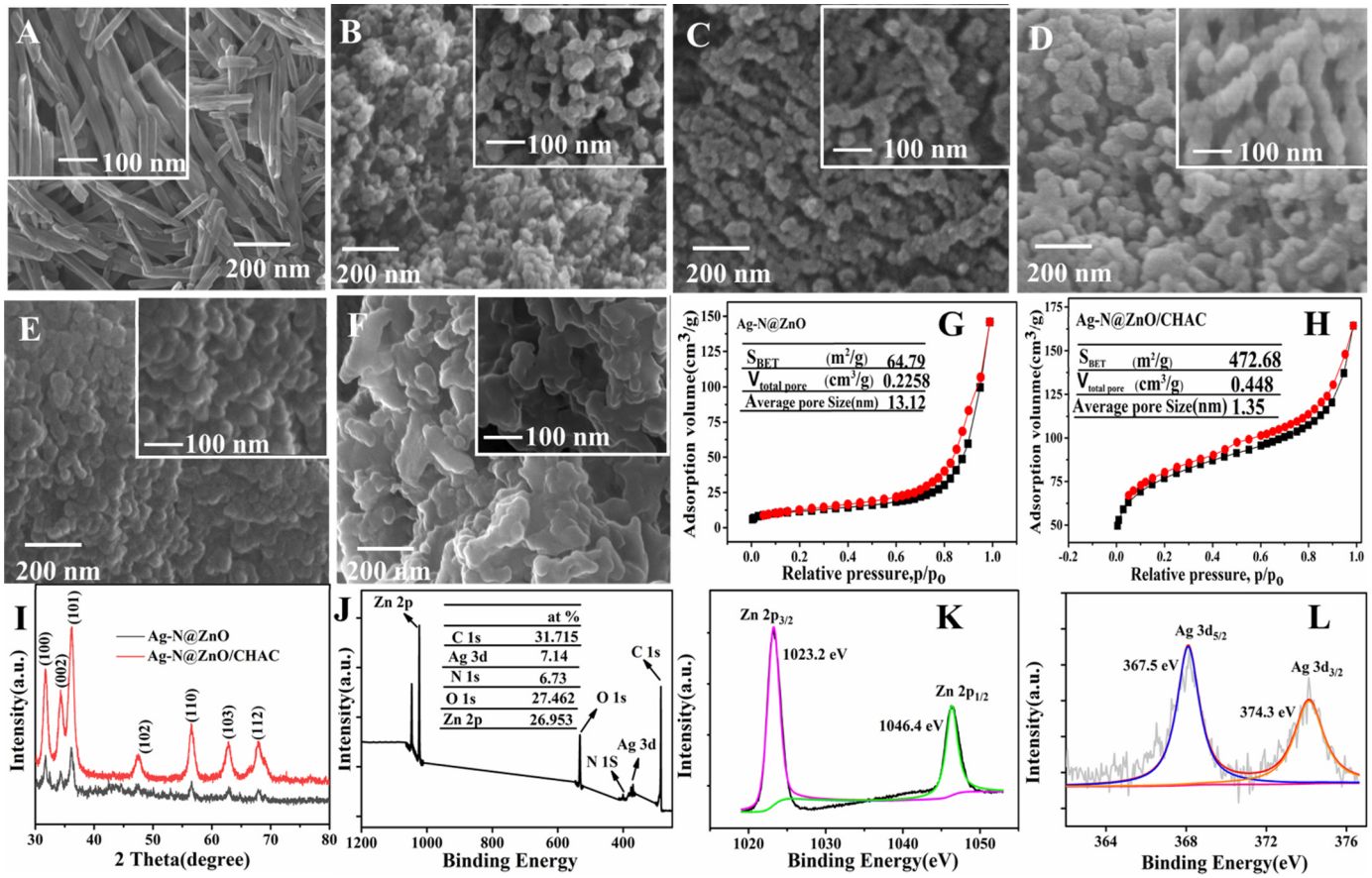

Fig. 2. SEM images of ZnO (A), Ag-N@ZnO (B), CHAC (C), Ag-N@ZnO/CHAC (D), DMMIP-Ag-N@ZnO/CHAC/GCE before (E) and after (F) extraction of CYP; N2 adsorption/desorption isotherms curves of Ag-N@ZnO (G), Ag-N@ZnO/CHAC (H), XRD patterns of Ag-N@ZnO and Ag-N@ZnO/CHAC (I); XPS spectra of Ag-N@ZnO/CHAC (J) Zn 2p (K) and Ag 2p (L).

N-ZnO (472.68 m^2 g^{-1}). The illustration shows that the total pore volume of Ag-N@ZnO/CHAC is twice larger than that of Ag-N@ZnO. XRD patterns of Ag-N@ZnO and Ag-N@ZnO/CHAC are shown in Fig. 2I, which agree well with the patterns of JCPDS cards (No. 36–1451). However, no apparent characteristic diffraction peaks of Ag and N were observed in the XRD patterns of all the prepared samples. Such results suggest that addition of Ag, N and CHAC has little effect on the plane of hexagonal wurtzite structure of ZnO, which could be attributed to the low doping amount. Similar results were also reported by Bhirud et al. (Bhirud et al., 2015). Moreover, the characteristic diffraction peak of CHAC was not detected in Ag-N@ZnO/CHAC, which is probably due to the amorphous carbon in CHAC has relatively low crystallinity and diffraction intensity (Ding et al., 2016). XPS spectra of Ag-N@ZnO/CHAC is shown in Fig. 2J. The C 1 s region exhibits main peak at 284.6 eV, which is derived from sp2 hybrid C-C in CHAC (Zhao et al., 2018). The peaks at approximately 530.8 eV were mainly attributed to lattice oxygen present in ZnO, which can also be seen from the percentage of zinc and oxygen (inset of Fig. 2J). Nitrogen doping into ZnO is confirmed by the obvious XPS signal of N 1s. The peaks at around 400.3 eV can be attributed to -Zn-N-O- or -O-Zn-N- (Muthulingam et al., 2015; X.Y. Zhang et al., 2015), indicating the substitution of nitrogen for some amounts of oxygen. The XPS spectrum of Zn in Ag-N@ZnO/CHAC in Fig. 2K shows the peaks of two different binding energies, which correspond to Zn 2p 3/2(1023.3 eV)and Zn 2p 1/2(1046.4 eV), implying that zinc atoms mainly exist as state of Zn^{2+} in the samples (Li et al., 2012). Fig. 2L exhibits the Ag 3d5/2 and 3d3/2 signals appeared at 367.5 eV and 374.5 eV with a splitting doublet of 7 eV. This indicates that Ag mainly exists in metallic Ag state on the surface of Ag-N@ZnO/CHAC (Liu et al., 2018).

3.2. Electrochemical characterization

Electrochemical behavior of the electrodes obtained at different preparation steps was investigated via CV (Fig. 3A) and EIS (Fig. 3B). It is evident that decoration of ZnO reduces the peak current compared to bare GCE, due to poor conductivity of ZnO. Introduction of Ag and N raised the conductivity and enlarged surface area of the electrode, resulting in the oxidation/reduction peak current increase. However, it is less conductive than the bare electrode. A significant increase in the peak current was observed with CHAC modified electrode, which could be attributed to the large surface area containing various oxygen moieties. In order to further promote the sensitivity of the electrode, Ag-N@ZnO was grafted with biomass activated carbon from coconut shell, which significantly increased the peak current of the modified electrode. peak current of CHAC/GCE is much higher than that of bare GCE, and Ag-N@ZnO/CHAC/GCE displays the highest signal response, which can be attributed to good conductivity and compatibility between CHAC and Ag-N@ZnO (Chaudhary et al., 2017). EIS trackes the impedance changes at electrode surface, of which the results are in consistent with those from CV tests. The ZnO-modified electrode yielded an extremely big semicircle, implying poor conductivity of the electrode. Resistance value of CHAC/GCE is about 78 Ω. By comparison, Ag-N@ZnO/GCE produced a small semicircle, suggesting that doping of Ag-N benefits electron migration effectively. The lowest R value (R = 64 Ω) was obtained at Ag-N@ZnO/CHAC/GCE, probably owing to the enlarged surface area and the improved electron transferring rate after integration of the hybrid material.

To explore the effect of dual monomers and single monomer in MIP preparation on sensor performance, the CV results of MIP prepared with

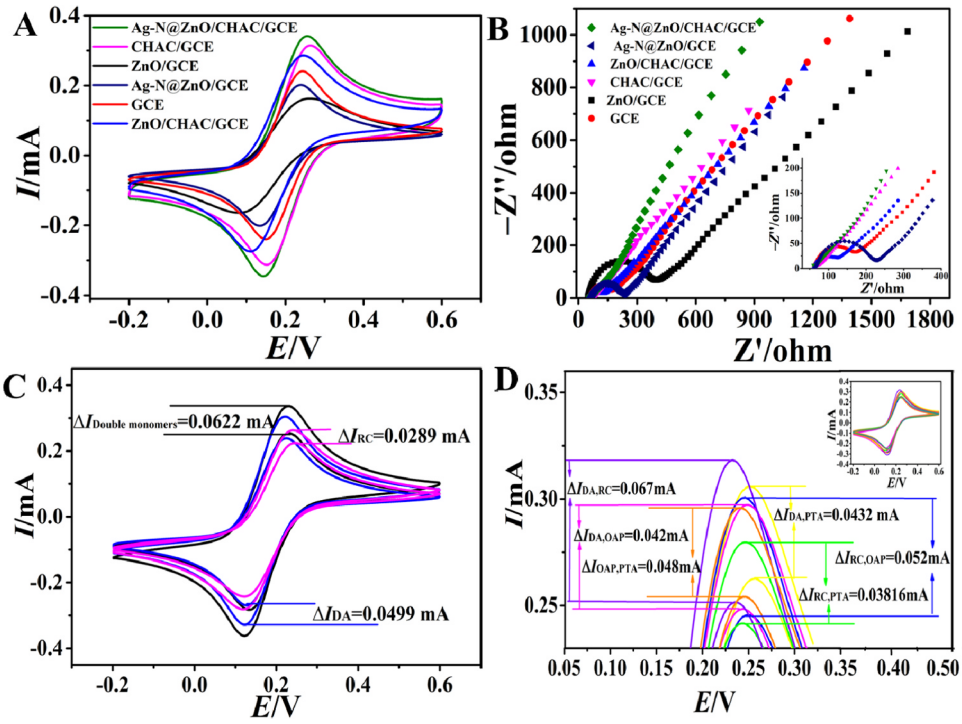

Fig. 3. Cyclic voltammograms (A) and EIS (B) of differently modified electrodes in solution of 5.0 mM $Fe(CN)_6^{3-/4-}$ containing 0.1 M KCl. The scan rate of CV was 0.10 V s^{-1} and the inset of (B) is EIS plots of bare GCE, ZnO/CHAC/GCE, Ag-N@ZnO/CHAC/GCE, CHAC/GCE and Ag-N@ZnO/GCE in their suitable coordinate range. Cyclic voltammograms (C) of double monomers and single monomer at a scan rate of 100 mV s p-value before and after binding with 5.0×10^{-11} M CYP; Current responses toward 8.0×10^{-11} M CYP by using a series of MIP electrodes prepared with different monomers.

dopamine and resorcinol as bifunctional monomers (DMMIP-Ag-N@ZnO/CHAC/GCE) and MIP prepared with dopamine (MIP_{DA}-Ag-N@ZnO/CHAC/GCE) or resorcinol (MIP_{RC}-Ag-N@ZnO/CHAC/GCE) alone as functional monomers were exhibited and compared in Fig. 3C. DMMIP-Ag-N@ZnO/CHAC/GCE was fabricated under the optimal concentration ratio of DA, RC and CYP (3:5:3). MIP_{DA}-Ag-N@ZnO/CHAC/GCE and MIP_{RC}-Ag-N@ZnO/CHAC/GCE were also prepared at the optimal ratio of functional monomer and template molecule at the molar ratio of 3:1. Besides, DMMIP-Ag-N@ZnO/CHAC/GCE displays the highest sensing response to CYP, which is about 1.25 times larger than that of MIP_{DA}-Ag-N@ZnO/CHAC/GCE and 2.15 times than that of MIP_{RC}-Ag-N@ZnO/CHAC/GCE. This may be due to the synergistic effect of dual monomers, which increases diversity of the types of blotting sites in MIP architecture and therefore enhances binding and affinity. The demonstration process is shown in Fig. S1.

The type of functional monomer has a significant influence on the functional groups produced in MIP framework and the interaction between template and MIP. PTA, DA, OAP and RC were set as the bifunctional monomers to find the highest imprinting effect toward CYP in a molar ratio of template to monomer (T: M: M) of 1:1.5:1.5 (1×10^{-3} M:1.5×10^{-3} M:1.5×10^{-3} M) with incubation time of 10 min. As shown in Fig. 3D, MIP with DA and RC as functional monomers had the maximum current response. It is due to the fact that DA and RC as functional monomers have multiple functional groups, thus high affinity binding sites can be obtained during imprinted process. At the same time, combination with bifunctional monomers has good synergistic effect, larger rigidity, uniform pore size and precise three-dimensional structure on electrode surface, which can increase the specific recognition ability of the imprinted molecule.

3.3. Optimization of experimental conditions

During MIP preparation, the ratio of template molecules to functional monomers will affect the imprinting sites, further influencing the binding ability to target substance. Inadequate functional monomer results in insufficient binding sites for CYP, while excessive amount of monomer produces non-imprinted sites and leads to non-specific binding.

Table 1
Analysis of variance for the response surface quadratic model for current response of DMMIP-Ag-N@ZnO/CHAC/GCE in probe solution after rebinding with 2×10^{-12} M CYP.

Source	Sum of squares	DF	Meansquare	F-Value	Prob > F	Remarks
Model	2.726×10^{-3}	9	3.011×10^{-3}	833.19	0.0011	Significant
A	3.168×10^{-5}	1	3.168×10^{-5}	30.45	0.0009	Significant
B	1.292×10^{-3}	1	1.292×10^{-3}	53.38	0.0002	Significant
C	9.430×10^{-4}	1	9.430×10^{-4}	25.31	0.0015	Significant
AB	1.266×10^{-4}	1	1.266×10^{-4}	19.64	0.0030	Significant
AC	5.112×10^{-5}	1	5.112×10^{-5}	13.17	0.0084	Significant
BC	1.405×10^{-5}	1	1.405×10^{-5}	0.38	0.5587	Nonsignificant significant
A^2	1.163×10^{-4}	1	1.163×10^{-4}	3.12	0.1206	Nonsignificant
B^2	2.311×10^{-6}	1	2.311×10^{-6}	0.062	0.8105	Nonsignificant
C^2	1.493×10^{-4}	1	1.493×10^{-4}	5.182	0.3247	Nonsignificant significant
Residual	3.1379×10^{-4}	7	1.032×10^{-4}	–	–	–
Lack of Fit	2.972×10^{-4}	3	9.908×10^{-5}	1.06	0.4583	Nonsignificant
Pure Error	1.659×10^{-5}	4	4.147×10^{-6}	–	–	–
Cor Total	3.039×10^{-3}	16	–	–	–	–

DF: degree of freedom.

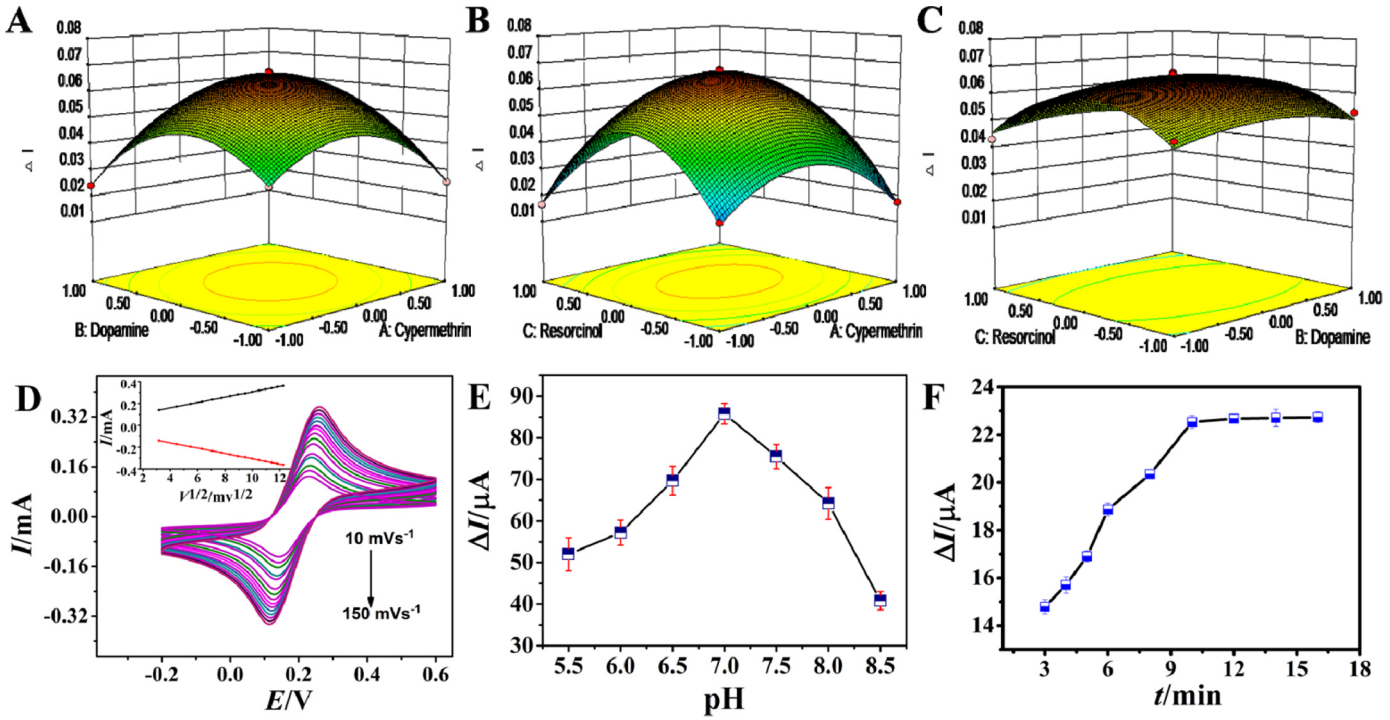

Fig. 4. Three dimensional response surface diagram of current response of cypermethrin to molecularly imprinted polymers prepared at different ratios: different proportions of template molecules and DA (A), different proportions of template molecules and RC (B), different proportions of dopamine and Resorcinol (C); Cyclic voltammograms of DMMIP-Ag-N@ZnO/CHAC/GCE at the scan rate from 10 to 200 mV s^{-1} (D). the inset of (D) is the anodic and the cathodic peak currents versus the square-root of the scan rate plot; Sensing responses toward 8×10^{-11} M CYP using MIP/GE prepared with varied pH values (E); Time course analysis of signal response of CYP at a concentration of 8×10^{-11} M (F). Error bars represent means ± the variation range of triplicates.

A three-level, three-factor Box–Behnken design was employed to determine the optimal proportion of template molecules and double monomers; the results are shown in Table S1, and the analysis of variance (ANOVA), goodness-of-fit and the adequacy of the regression model are summarized in Table 1. The high model F-value and the low P-value indicates the level of confidence of the selected model [20]. The model F-value of 833.19 and the associated low p-value ($p < 0.01$) implied that the model was highly statistically significant. The fact that P-value is more than F for 0.05 indicates that the factor is significant. The models of AB, AC, A, B and C are significant factors, which show the importance and validity of the independent variables selected in the experiment. Since A^2, B^2, C^2, and BC are not significant factors, the interaction between the template itself, the monomer itself and the polymerization between different monomers during molecular imprinting preparation has little effect on the formation of molecular imprinting sites. The regression equation was plotted, and the shape of the fitted curved surface was investigated. The three-dimensional analysis of response surface (Fig. 4) shows the effect of MIPs prepared from the template molecule and the functional monomer at different ratios on the current response toward the same concentration of CYP (8×10^{-11} M). The shape of contour plots indicates whether the mutual interactions between independent variables are significant.

In Fig. 4A, MIP was prepared with the varied amounts of CYP and DA but the fixed concentration of RC (4 M). The response of the corresponding sensors to CYP gradually increases with the increase of the concentrations of CYP and DA until it reaches the highest value of 0.0679 mA. Further increase in CYP and DA concentration leads to a decrease in the response. Similar observation was found in Fig. 4B, where the molecules with varied amounts were CYP and RC and the concentration of DA was fixed at 3 M. By contrast, when the amount of CYP (2 M) was fixed and the amounts of DA and RC were varied, the change of the sensor response was smaller than the former two conditions (Fig. 4C). Furthermore, contour line maps were plotted and presented in Fig. S3, which give rise to the same conclusion. A more detailed specify is shown in Table 1, where the significance level of different factors was provided.

In order to get the optimal ratio of template to bi-monomer, the experimental data in Table S1 were analyzed by multiple regression analysis and the following second-order polynomial equation was obtained:

$$\begin{aligned}\Delta I &= 0.055 + 1.325 \times 10^{-3}A + 3.813 \times 10^{-3}B - 5.375 \times 10^{-4}C \\ &\quad + 0.014AB + 0.011AC + 2.700 \times 10^{-3}BC^{-6}0.190 \times 10^{-3}A^2 \\ &\quad - 0.015B^2 - 0.021C^2\end{aligned}$$

Based on this equation, the optimal ratio of template molecules to functional monomers is 3:8, where the ratio of DA to RC is 3:5.

The effect of scan rate of MIP/Ag-N@ZnO/CHAC/GCE was investigated by CV (Fig. 4D). The absolute values of the oxidation peak currents increase linearly with the square root of scan rate in the range from 10 to 150 mV s^{-1}, revealing a diffusion-controlled mechanism at the sensor surface.

pH is an important factor impacting sensor performance. The electrochemical behavior of MIP/Ag-N@ZnO/CHAC/GCE in different polymerization solutions with pH values ranging from 2.0 to 8.0 was studied. It was found that ΔI increases quickly when the pH value increased from 5.5 to 7.0. However, when the pH value increased from 7.0 to 8.5, the current drops rapidly (Fig. 4E). Therefore, the optimal pH value is set at 7.0.

As shown in Fig. 4F, the signal response of CYP increased significantly with the increase of incubation time within 3–10 min. However, no apparent change was found after 11 min, which may be due to saturation of binding sites. Hence, 10 min was chosen as the optimal incubation time.

3.4. Sensing performance of DMMIP-Ag-N@ZnO/CHAC/GCE

The relationship between CYP concentration and current response is studied by CV at DMMIP-Ag-N@ZnO/CHAC/GCE under the optimum condition. As shown in Fig. 5A, the corresponding linear regression

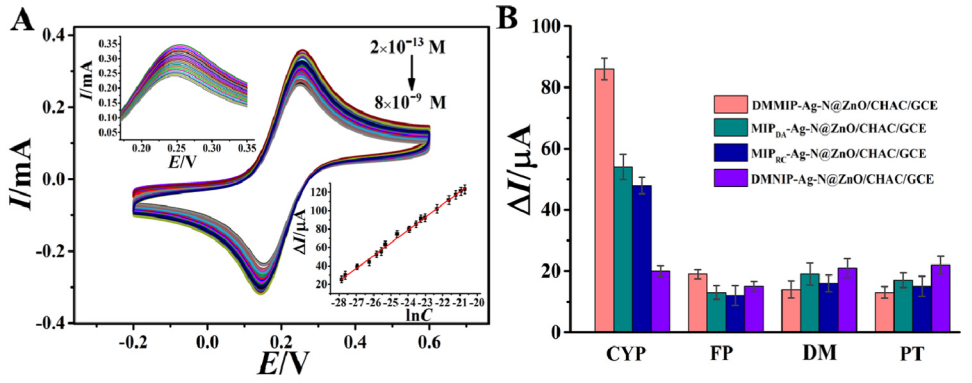

Fig. 5. Cyclic voltammograms of DMMIP-Ag-N@ZnO/CHAC/GCE in probe solution after rebinding with CYP in the concentration range of 2×10^{-13}~8×10^{-9} M The top left inset shows partially amplified cyclic voltammograms, and the bottom-right inset is the calibration curves correlating ΔI with the logarithm of concentration of CYP (ln$C$) (A); Comparison of sensing responses for CYP and its analogs at the concentration of 6×10^{-11} M by using DMMIP-Ag-N@ZnO/CHAC/GCE, MIP_{DA}-Ag-N@ZnO/CHAC/GCE, MIP_{RC}-Ag-N@ZnO/CHAC/GCE and DMNIP-Ag-N@ZnO/CHAC/GCE (B).

equation is ΔI (μA) = 13.804ln$C$ + 410.30 (R^2 = 0.9969) in the concentration range of 2×10^{-13}–8×10^{-9} mol L^{-1} with the detection limit estimated to be 3.4×10^{-13} mol L^{-1} (S/N = 3). Compared with the values reported by other research groups using chemically modified electrochemical sensors and biosensors for CYP analysis (Table S2), it is obvious that our presented DMMIP-Ag-N@ZnO/CHAC/GCE features a relatively wide linear range and the lowest detection limit.

The selectivity of DMMIP-Ag-N@ZnO/CHAC/GCE, MIP_{DA}-Ag-N@ZnO/CHAC/GCE, MIP_{RC}-Ag-N@ZnO/CHAC/GCE, DMNIP-Ag-N@ZnO/CHAC/GCE were studied in 1×10^{-11} M CYP coexisting with its structural analogs FP, DM and PT as shown in Fig. 5B. The responses of the MIP-sensor to the analogs were significantly lower than that to CYP. Besides, compared with the MIP-sensor, the response from non-imprinted polymer modified electrode to CYP is low, and there was no significant difference among the detection of all analyte. These results proved that nanocavities in MIP network, which were created during electropolymerization and template-extraction procedure, impart selectivity to the sensor due to the steric and structural matching between MIP and template molecules. The largest sensing response was obtained with DMMIP-Ag-N@ZnO/CHAC/GCE, which can be attributed to the existence of dual functional monomers providing diverse recognition sites. Compared with NIP sensor, both DMMIP sensor and MIP sensor have significantly higher responses in detecting CYP, indicating the existence and importance of imprinting effect. *T*-test also confirms significant difference in sensor responses of DMMIP-Ag-N@ZnO/CHAC/GCE to CYP and its analogs with a significant level of 0.01.

3.5. Verification of the established method

CYP at three different concentrations (2×10^{-12}, 4×10^{-12} and 6×10^{-12} M) were measured in triplicate using the same sensor. The relative standard deviation (RSD) for three replicate measurements was 2.1%, reflecting that the sensor possesses excellent repeatability. The same concentration (6×10^{-13} M) of CYP was continuously detected by the prepared sensor for 20 days. During this period, the sensor was stored at room temperature, and the obtained RSD was 3.7%. These data indicate that the sensor has good stability, which can be attributed to the mechanical and chemical stability of both Ag-N@ZnO/CHAC and MIP film.

3.6. Real samples analysis

To verify the feasibility of DMMIP-Ag-N@ZnO/CHAC/GCE for real sample analysis, the sensor was employed to determine CYP in soil, mackerel, crayfish and water. Determination of CYP in these samples was evaluated by standard addition method. The results in Table S3 reveal good accuracy with recoveries ranging from 96.21% to 100.43%. RSD is less than 8.89% verifying that the prepared sensor can be utilized for CYP determination in complex sample with qualified accuracy and precision.

4. Conclusions

This work describes a novel hybrid electrochemical sensor for highly selective and sensitive detection of CYP. To our knowledge, this is the first report on Ag-N@ZnO/CHAC-coated GCE with the combination of double-monomer MIP film as a promising sensor. In the composite modification membrane, the uniformly dispersed Ag-N@ZnO/CHAC elevates electron transfer rate at the electrode/electrolyte interface and provides enlarged surface area for MIP modification. The MIP film, which was in situ electrochemically prepared, contains dual monomers in its polymeric skeleton and affords the sensor with increased diversity of the types of blotting sites in MIP architecture and enhance binding and affinity by synergistic effects of different monomers. Reliability and applicability of the sensor was proved by detecting CYP in real samples. The DMMIP-Ag-N@ZnO/CHAC composite illuminates an good strategy to easily prepare the title sensor with good sensitivity and selectivity. It is expectable that the dual-monomer MIP sensor will play an important role in analysis field and serve determination of numerous biological and chemical targets of interest.

Acknowledgements

The project financially supported by National Natural Science Foundation of China (81773680 and 21575089) and Scientific Research Foundation for Changjiang Scholars of Shihezi University (CJXZ201501).

Declaration of interests

The authors declare that they have no known competing financial interests or personal relationships that could have appeared to influence the work reported in this paper.

Conflicts of interest

There are no conflicts to declare.

Appendix A. Supporting information

Supplementary data associated with this article can be found in the online version at doi:10.1016/j.bios.2018.12.002.

References

Alongi, J., Pošković, M., Frache, A., Trotta, F., 2010. Polym. Degrad. Stabil. 95 (10), 2093–2100.
Alvau, M.D., Tartaggia, S., Meneghello, A., Casetta, B., Calia, G., Serra, P.A., Polo, F., Toffoli, G., 2018. Anal. Chem. 90 (10).
Bhirud, A., Sathaye, S., Waichal, R., Park, C.J., Kale, B., 2015. J. Mater. Chem. A 3 (33), 17050–17063.
Bougrine, A., Hichou, A.E., Addou, M., Ebothé, J., Kachouane, A., Troyon, M., 2003. Mater. Chem. Phys. 80 (2), 438–445.

Capoferri, D., Alvarez-Diduk, R., Del, C.M., Compagnone, D., Merkoçi, A., 2018. Anal. Chem. 90 (9), 5850–5856.
Chaudhary, M., Doong, R.A., Kumar, N., Tseng, T.Y., 2017. Appl. Surf. Sci. 420, 118–128.
Chen, M.M., Wang, Y., Cheng, S.B., Wen, W., Zhang, X., Wang, S., Huang, W.H., 2018. Anal. Chem. 90 (8), 5075–5081.
Ding, S.Y., Yi, J., Li, J.F., Ren, B., Wu, D.Y., Panneerselvam, R., Tian, Z.Q., 2016. Nat. Rev. Mater. 1, 16021–16036.
GóMez-Gimã©Nez, B., Llansola, M., Cabrera-Pastor, A., Hernã, N.-R.V., Agustã, A., Felipo, V., 2017. Acs Chem. Neurosci. 9 (2), 369–380.
Geng, H., Kong, S., Wang, Y., 2014. J. Mater. Chem. A 2 (36), 15152–15158.
Gui, R., Jin, H., Guo, H., Wang, Z., 2018. Biosens. Bioelectron. 100, 56–70.
Gupta, B.D., Shrivastav, A.M., Usha, S.P., 2016. Sensors 16 (9), 1381.
Habaue, S., Satonaka, T., Nakano, T., Okamoto, Y., 2004. Polym. Chem. 45 (15), 5095–5100.
Ibrahim, A.A., Hwang, S.W., Dar, G.N., Kim, S.H., Abaker, M., Ansari, S.G., 2015. Sci. Adv. Mater. 7 (7), 1241–1246.
Kaur, B., Erdmann, C., Daniels, M., Dehaen, W., Rafiński, Z., Radecka, H., Radecki, J., 2017. Anal. Chem. 89 (23), 12756–12763.
Li, S.S., Zhou, W.Y., Li, Y.X., Jiang, M., Guo, Z., Liu, J.H., Huang, X.J., 2017. Anal. Chem. 90 (2), 1263–1272.
Li, W.J., Kong, C.Y., Qin, G.P., Ruan, H.B., Yang, T.Y., Meng, X.D., Zhao, Y.H., Liang, W.W., Fang, L., 2012. Sci. Sin. 42 (8), 819–826.
Li, Y., Liu, J., Zhang, Y., Gu, M., Wang, D., Dang, Y.Y., Ye, B.C., Li, Y., 2018. Biosens. Bioelectron. 106, 71–77.
Li, Y., Song, H., Zhang, L., Zuo, P., Ye, B.C., Yao, J., Chen, W., 2016a. Biosens. Bioelectron. 78, 308–314.
Li, Y.C., Zhang, L., Liu, J., Zhou, S.F., Al-Ghanem, K.A., Mahboob, S., Ye, B.C., Zhang, X., 2016b. Rsc Adv. 6 (49), 43724–43731.
Liu, Y., Chai, X., Cai, X., Chen, M., Jin, R., Ding, W., Zhu, Y., 2018. Angew. Chem. Int. Ed. 57 (31), 9775–9779.
Madhu, R., Veeramani, V., Chen, S.M., 2014. Sens. Actuators B Chem. 204, 382–387.
Muthulingam, S., Lee, I.H., Uthirakumar, P., 2015. J. Colloid Interface Sci. 455, 101–109.
Naganathan, D., Thangamani, P., Selvam, T., Narayanasamy, T., 2018. Microchim Acta 185 (2), 96.
Ng, K.L., Khor, S.M., 2017. Anal. Chem. 89 (18), 10004–10012.
Ramstroem, O., Andersson, L.I., Mosbach, K., 1993. J. Org. Chem. 58 (58), 7562–7564.
Shafer, T.J., Meyer, D.A., Crofton, K.M., 2005. Environ. Health Perspect. 113 (2), 123–136.
Shin, Y., Lee, J., Lee, J.H., Lee, J., Kim, E., Liu, K.H., Lee, H.S., Kim, J.H., 2018. J. Agric. Food Chem. 66 (13), 3550–3560.
Si, X., Wei, Y., Wang, C., Li, L., Ding, Y., 2018. Anal. Methods 10 (17).
Suematsu, K., Watanabe, K., Tou, A., Sun, Y., Shimanoe, K., 2018. Anal. Chem. 90 (3), 1959–1966.
Tang, A.X., Liu, H., Liu, Y.Y., Li, Q.Y., Qing, Y.M., 2017. J. Agric. Food Chem. 65 (43), 9412–9418.
Wang, C., Ye, X., Wang, Z., Wu, T., Wang, Y., Li, C., 2017. Anal. Chem. 89 (22), 12391–12399.
Wang, Y.W., Liu, Y.L., Xu, J.Q., Qin, Y., Huang, W.H., 2018. Anal. Chem. 90 (10), 5977–5981.
Wei, Y., Zeng, Q., Bai, S., Wang, M., Wang, L., 2017. Acs Appl. Mater. Int. 9 (50), 44114–44123.
West, S.D., 1997. J. Agric. Food Chem. 45 (8), 3107–3113.
Wu, Z., Guo, W.J., Bai, Y.Y., Zhang, L., Hu, J., Pang, D.W., Zhang, Z.L., 2017. Anal. Chem. https://doi.org/10.1021/acs.analchem.7b03281.
Wu, L., Liu, F., Wang, G., Guo, Z., Zhao, J., 2016. RSC Adv. 6 (1), 464–471.
Zhang, C., Xiong, D., Xu, S., Ouyang, W., Wang, L., Chu, P.K., 2018a. Mater. Lett. 222, 25–28.
Zhang, H., Yao, R., Wang, N., Liang, R., Qin, W., 2018b. Anal. Chem. 90 (1), 657–662.
Zhang, Q., Li, L., Qiao, Z., Lei, C., Fu, Y., Xie, Q., Yao, S., Li, Y., Ying, Y., 2017. Anal. Chem. 89 (22), 12145–12151.
Zhang, W., Li, B., Chen, L., Wang, Y., Gao, D., Ma, X., Wu, A., 2014. Anal. Methods 6 (7), 2066–2071.
Zhang, X.Y., Deng, Y.J., Liu, J.K., Lu, Y., Yang, X.H., 2015a. J. Colloid Int. Sci. 459, 1–9.
Zhang, Y., Peng, Z., Ye, B.C., 2015b. Biosens. Bioelectron. 68, 14–19.
Zhang, Z., Li, L., 2018. J. Sep. Sci. 41 (11), 2479.
Zhao, J., Zhao, D., Chen, J., Tian, Y., Zong, Q., Fan, Y.C., Nie, C.K., Liu, B.Z., 2018. Optik 161, 342–347.
Zhao, W.R., Kang, T.F., Lu, L.P., Shen, F.X., Cheng, S.Y., 2017. J. Electrochem. Chem. 786.
Zhou, J.W., Zou, X.M., Song, S.H., Chen, G.H., 2018. J. Agric. Food Chem. 66 (6), 1307–1319.